

<https://doi.org/10.1038/s43247-024-01470-z>

Australia's 2019/20 Black Summer fire weather exceptionally rare over the last 2000 years

Check for updates

Danielle G. Udy ^{1,2,3,4} ✉, Tessa R. Vance ³, Anthony S. Kiem ⁵, Neil J. Holbrook ^{1,2} & Nerilie Abram ^{6,7,8}

Australia's record-breaking 2019/20 Black Summer fire weather resulted from a combination of natural and anthropogenic climate factors, but the full range of natural variability in fire weather is unknown. We reconstruct southeast Australian fire weather over the Common Era based on an East Antarctic ice core sea-salt aerosol record. This record reflects the Southern Ocean synoptic-scale weather patterns and Antarctic stratospheric polar vortex strength that pre-condition elevated fire danger over southeast Australia. We show that the (a) intensity of the 2019/20 fire weather was unprecedented since 1950 and (b) frequency of above average fire weather seasons from 2010–2020 has only occurred once since 1950 (over 1977–1987), but there are analogues for similar extreme fire danger caused by natural variability in the 2000-year reconstruction. This highlights the need for fire risk mitigation that considers the full range of plausible natural variability in Australia's fire weather as well as anthropogenic forcing.

Wildfire activity in many parts of the world is escalating as climatic conditions become more conducive to frequent and extreme fire weather^{1,2}. Fire weather, which is characterised by high temperatures, low humidity, and strong winds, plays a key role in determining wildfire activity and severity. Fire weather is independent of other factors that influence fire activity including vegetation type, topography and fire management policies^{2–6}. Since ~2000, the frequency and severity of fire weather globally has increased due to increasing temperatures and decreasing relative humidity⁷ and is projected to escalate with each additional increment of anthropogenic warming². The increased frequency and severity of fire weather has contributed to many recent wildfire disasters, such as in Chile and Portugal in 2017^{8,9}, Greece in 2018¹⁰, California in 2018¹¹ and 2020¹², Australia in 2019–20^{13,14}, and widespread fires across North America and Europe in 2023¹⁵.

The 2019/20 Black Summer (September 2019–February 2020) fire disaster in southeast Australia was unprecedented in historical experience^{3,14,16}. The 2019/20 fires were unmatched in observational records in their radiative power, the area they burned, and the number of fires that developed into extreme pyro-convective events¹⁴. These fires resulted in 33

direct fatalities, over 80% of the Australian population exposed to dangerous air pollution, and 417 excess deaths (i.e. higher than expected deaths)¹⁷. The extreme fire activity over the Black Summer was driven by a combination of multiple factors, including the compounding influences of severe multi-year drought¹⁸, alignment of fire-promoting phases of multiple modes of climate variability, and long-term increases in temperature and vapour pressure deficit from anthropogenic greenhouse gas emissions^{14,19–21}.

Disentangling the relative influence of natural variability from anthropogenic climate change on southeast Australian fire weather remains challenging due to the large and complex interannual climate variability^{22–26} in this region, combined with short (post-1950) observational records of fire weather^{14,27}. Elevated fire weather across southeast Australia is strongly preconditioned by reduced seasonal rainfall and increased temperature, and the year-to-year variability of these is modulated by the strength of the Antarctic stratospheric polar vortex and large-scale modes of climate variability¹⁴. Austral springtime Antarctic stratospheric polar vortex weakening events, a negative Southern Annular Mode (SAM), the warm phase of El Niño Southern Oscillation (ENSO; El Niño), and positive Indian Ocean Dipole (IOD) conditions are all associated with elevated fire weather hazard

¹Institute for Marine & Antarctic Studies, University of Tasmania, Hobart, TAS 7004, Australia. ²ARC Centre of Excellence for Climate Extremes, University of Tasmania, Hobart, TAS 7004, Australia. ³Australian Antarctic Program Partnership, Institute for Marine & Antarctic Studies, University of Tasmania, Hobart, TAS 7004, Australia. ⁴Australian Centre for Excellence in Antarctic Science, University of Tasmania, Hobart, TAS 7004, Australia. ⁵Centre for Water, Climate and Land, College of Engineering, Science and Environment, University of Newcastle, Callaghan, NSW 2308, Australia. ⁶Research School of Earth Sciences, Australian National University, Canberra, ACT 2601, Australia. ⁷ARC Centre of Excellence for Climate Extremes, Australian National University, Canberra, ACT 2601, Australia. ⁸Australian Centre for Excellence in Antarctic Science, Australian National University, Canberra, ACT 2601, Australia. ✉e-mail: danielle.udy@utas.edu.au

over southeast Australia (Supplementary Fig. 1)^{14,19,22,23,28,29}. These large-scale climate states favour synoptic-weather conditions associated with increased daytime maximum temperatures, drier conditions, strong winds, and wind direction changes (e.g. summer cold fronts)^{14,28,30,31}. Strong summer cold fronts have contributed to many devastating fire events in Australia, including the 1983 Ash Wednesday^{32,33}, 2003 Canberra fires³⁴, 2009 Black Saturday fires^{30,35,36} and the 2019/20 Black Summer fires³¹. Accurate representation of these synoptic-scale dynamics and extremes in climate models remains challenging^{19,20}. In addition to interannual variability in fire weather, there has also been a shift towards more extreme fire weather over southeast Australia since the late 1990s^{3,16,23}, which has been associated with record vapour pressure deficit³⁷ and attributed primarily to increasing temperatures^{1,27}. However, the emergence of severe fire weather beyond the observed range of variability in the region most heavily impacted by the 2019/20 fires (coastal and alpine region of southeast Australia; Supplementary Fig. 1) is less clear and sensitive to methods and time periods used. An attribution study²⁰ found that temperature increases had resulted in at least a 30% increase since 1979 in severe fire weather over the region impacted by the 2019/20 fires, while other studies have reported no significant trend in this region^{2,19,38,39}.

Past periods of enhanced fire activity, drought, and elevated temperatures provide valuable context to distinguish the relative influence of natural variability and anthropogenic forcing on recent fire weather extremes. However, the temporal and spatial spread of suitable palaeoclimate archives for reconstructing fire weather is limited across Australia. The majority of Australian rainfall and temperature proxy records with annual temporal resolution extend back only ~500 years^{40,41}. Lower temporal resolution records, including speleothems and lake sediments, suggest the recent centuries (~1400–1900CE) were wetter and cooler, and therefore had reduced fire hazard, compared to earlier centuries in the Common Era (pre-

1250CE)^{42–44}. Reconstructing past fire weather (i.e. hazard) from fire activity is also difficult due to the combined influence of climate, vegetation, and human activity on fire occurrence. Most palaeo-fire archives in Australia are direct proxies of fire activity, such as sedimentary charcoal and tree scars, rather than of fire weather. This is an important distinction as certain time periods could have elevated fire weather even if no major fire activity occurred, due to either no ignition source or fuel being recently burnt. The severity and frequency of past fire activity was also influenced by vegetation type, fuel loads and land management decisions, including the ignition or suppression of fire. The disruption of Indigenous cultural burning practices in Australia following colonial settlement has been argued to have increased shrub cover and may have exacerbated the intensity of the Black Summer fires beyond expectations from climate variability and change alone⁴⁵.

A reconstruction of fire weather for southeast Australia would complement existing temperature, rainfall, and charcoal records and provide important context for recent observed increases in fire weather frequency and severity. Here we use an annually resolved ice core record from Law Dome (East Antarctica) to reconstruct the past fire weather hazard in southeast Australia over the Common Era (1–2016CE) (Fig. 1a). Law Dome is a small coastal ice cap in Wilkes Land, East Antarctica. The region is dominated by frequent incursions of extratropical cyclones from the Southern Ocean^{46,47}. This results in a high annual snowfall accumulation rate (~1.5 m/year) that preserves seasonal to annual resolution climate signals with minimal annual dating error over the Common Era^{48–52}. Sea-salt aerosols preserved in the Law Dome ice core record over austral summer reflect an oceanic wind proxy of atmospheric circulation changes over the Indo-Pacific sector of the Southern Ocean^{49,53,54}. Sea-salt aerosol production from the ocean surface increases exponentially once the surface wind speed exceeds 3 ms⁻¹⁵⁵, with the majority (98%) of sea-salt aerosol particles falling back into the ocean close to the source⁵⁶. Of the remaining ~2% of particles

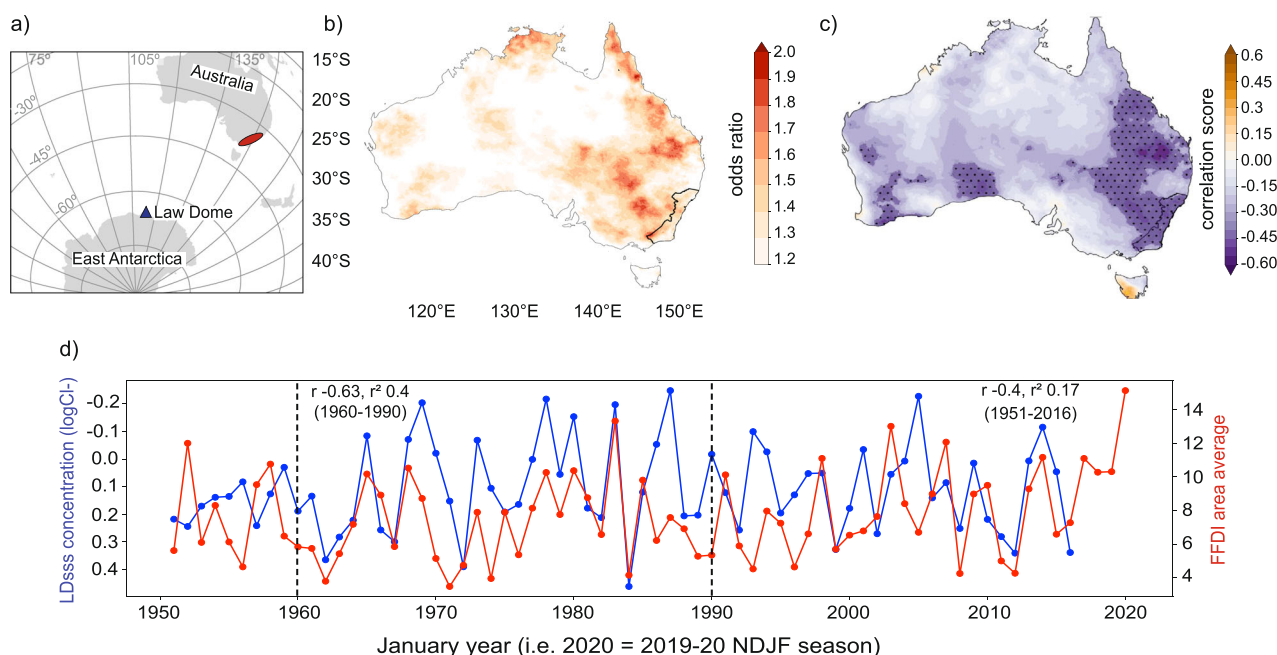


Fig. 1 | Seasonal relationship between Law Dome summer sea-salt (LDss) and Australian fire weather over November to February (NDJF). **a** Map of the study region showing the location of Law Dome (blue triangle) and focus region of southeast Australia (red ellipse). **b** Odds ratio of the probability of occurrence of high fire weather hazard days (Forest Fire Danger Index > 90th percentile (1951–2016)) in late spring-summer during 22 low-sea salt aerosol concentration seasons (LDss lower tercile < 33% between 1951–2016) vs 45 non-low-sea salt aerosol concentration seasons in the ice core. **c** Pearson correlation between LDss and Australian seasonal average (NDJF) Forest Fire Danger Index (FFDI) between 1950/51 – 2015/16

16. Dots indicate significance accounting for temporal and spatial autocorrelation (i.e. false discovery rate). The black area outline indicates the region used for area average calculation in **d**, and is based on the confluence of the region affected by the Black Summer fires and the region where LDss has a strong connection to Australian FFDI. **d** Timeseries comparison between area-averaged FFDI over southeast Australia (area marked on **b/c**) and inverted LDss concentration ($\mu\text{Eq L}^{-1}$). The correlation and regression score between LDss and area average FFDI over two time periods are shown; 1951–2016 and 1960–1990.

that are exported away from the original source location, only ~4% of the particles are comprised of submicron particles (<1 μm) that are small enough to undergo long-range transport and act as cloud condensation nuclei⁵⁶. Variability in the production and transport of these submicron particles to the Law Dome region is related to regional atmospheric circulation, with elevated sea-salt aerosol concentrations at the ice core site associated with the incursion of cyclonic systems^{46,49}. Specifically during austral summer, increased sea-salt aerosol deposition at Law Dome is associated with a regional, and notably asymmetric contraction of the mid-latitude westerlies which reflects a component of positive SAM conditions in the southern Indian Ocean^{47,54}. Decreased sea-salt aerosol deposition at Law Dome is associated with an equatorward shift in the mid-latitude westerlies, consistent with negative SAM conditions⁵⁴.

To establish the suitability of sea-salt aerosol deposition at Law Dome in representing fire weather in southeast Australia we first examine the relationship of Law Dome ice core sea-salt concentration⁵¹ to observational records of the Australian Forest Fire Danger Index (FFDI)²⁷. We then use an existing daily synoptic typing dataset of the southern Indian Ocean⁴⁷ to demonstrate a synoptic-scale weather connection that imprints on sea-salt aerosol deposition in snowfall at Law Dome as well as fire weather across southeast Australia. The synoptic typing dataset consists of nine 'types' and was constructed using a self-organising maps (SOMs) algorithm on 500hPa geopotential height daily anomalies from ERA-Interim reanalysis data⁴⁷ (Methods). Using this synoptic typing dataset, Udy et al.⁵⁴ established a synoptic-scale connection between the Law Dome summer sea-salt record and November to February rainfall variability over eastern Australia. This study extends the established synoptic connection between Law Dome and eastern Australia to reconstruct fire weather variability over the Common Era, enabling the significance of recent increases in fire weather hazards to be evaluated in the context of natural variability.

Results and Discussion

Synoptic connection between Law Dome and Australian fire weather hazard

The chance of high fire danger days occurring between November and February over southeast Australia is twice as likely during years with low deposition of sea-salt aerosol in snowfall at Law Dome (Fig. 1b). Decreased concentrations of sea-salt aerosol in the Law Dome record and elevated fire weather hazard over southeast Australia during late austral spring-summer (Fig. 1c, d) are both generated by synoptic-scale weather conditions that represent an equatorward shift in the mid-latitude westerly winds^{28,47,54}. This supports the significant correlation between the summer sea-salt concentration in the Law Dome ice core and the November-February FFDI averaged over the forested east coast and alpine region of southeast Australia that was affected by the Black Summer fires ($r_{\text{Pearson}} = +0.41$, $p < 0.01$, 1951–2016; Fig. 1d).

The conditions that lead to decreased summer sea-salt concentration in the Law Dome ice core record and elevated fire weather seasons due to the frequent summer cold front passage over southeast Australia are characterised by negative atmospheric pressure anomalies over southern Australia (extra-tropical cyclones and cold-fronts) and positive pressure anomalies over East Antarctica (strengthened Antarctic anticyclone) (Fig. 2b-i). This pressure anomaly pattern, consistent with negative SAM conditions⁴⁷, decreases the westerly wind strength and associated sea-salt aerosol production near the East Antarctic coastline⁵⁴ and doubles the chance of high fire danger days over southeast Australia due to the passage of cold fronts^{47,54} (Fig. 2b-ii). The passage of cold fronts and associated pre-frontal trough over southeast Australia during late austral spring-summer is well known to be associated with dry, hot, and windy conditions, elevating fire weather hazard^{30,31,35}. For example, increased frequency of cold front passage during the 2019/20 Black Summer significantly increased the likelihood of severe fire weather days³¹.

The location of cold fronts and surrounding weather systems influences the region of elevated fire hazard over southeast Australia, while at the same time modulating the connection to East Antarctica by varying the

concentration of aerosol sea-salt in snowfall at Law Dome. Four synoptic types (SOM1, SOM3, SOM7, SOM9) from the grouped synoptic conditions described in Udy et al.⁴⁷, are associated with elevated fire hazards across southeast Australia (Fig. 2-iii), however only two (SOM3, SOM7) of these are related to variability in the Law Dome sea-salt aerosol concentration record⁵⁴. All four of these synoptic types feature negative pressure anomalies either over southeast Australia or in the Great Australian Bight, reflecting cold fronts and low-pressure systems⁴⁷. Synoptic conditions characterised by negative pressure anomalies located further north than usual in austral spring/summer (SOM3) or in the Tasman Sea (SOM1) are associated with elevated fire weather and up to double the chance of a high fire danger day (FFDI >90th percentile) occurring over a broad area of eastern Australia (including the 2019/20 fire region) (Fig. 2a, b-ii/iii). The synoptic conditions associated with SOM3 are reflected in reduced sea-salt concentrations in the Law Dome ice core record⁵⁴. However, during SOM1 conditions the connection between Law Dome summer sea-salt and fire weather over eastern Australia breaks down due to the synoptic conditions around East Antarctica causing no significant difference in sea-salt aerosol deposition at Law Dome⁵⁴. This synoptic breakdown explains why some high fire danger events associated with SOM1 conditions including the Black Christmas fires⁵⁷ during the 2001/02 summer season are not reflected in the seasonal Law Dome summer sea-salt record.

Synoptic conditions characterised by negative pressure anomalies located in the Great Australian Bight (SOM7/SOM9), are associated with elevated fire weather and up to double the chance of a high fire danger day occurring over western Victoria and Tasmania (Fig. 2c, d-ii/iii). SOM7 conditions are more strongly connected to increased sea-salt aerosol deposited at Law Dome than SOM9 and represents an asymmetric contraction of the mid-latitude westerly winds towards the Law Dome coastline that increases sea-salt aerosol production near East Antarctica⁵⁴. SOM7 is characterised by surface anticyclones to the southwest and southeast of Australia, a surface cold front approaching southeast Australia, and an upper-level trough over eastern Australia^{47,54}. This pressure anomaly pattern, consistent with asymmetric positive SAM conditions⁴⁷, is often associated with Rossby wave-breaking events⁵⁸ which support the dipole fire hazard observed between subtropical and mid-latitude regions of eastern Australia (Fig. 2c-iii). Rossby wave-breaking events in this region lead to the co-occurrence of elevated fire weather over southwest Victoria and Tasmania and widespread rainfall over subtropical eastern Australia^{58,59}. The severe fire weather over southeast Australia is associated with a surface cold front/pre-frontal trough that drives dry and warm conditions from inland Australia to the southeast via north-westerly winds^{30,32,36,58}, elevating fire weather hazard and the chance of high fire danger over the mid-latitudes (Fig. 2c-iii). The widespread rainfall over subtropical eastern Australia decreases fire weather hazard (Fig. 2c-iii) and is driven by the Tasman Sea anticyclone and upper-level low pressure which delivers moist surface easterly winds^{54,60} and enhanced vertical uplift over the east coast^{58,60–62}.

Influence of the Antarctic stratospheric polar vortex

The Antarctic stratospheric polar vortex strength and seasonal breakdown timing influences the phase and persistence of SAM, with weakened polar vortex years supporting persistent negative SAM conditions and elevated fire weather hazards in southeast Australia between October and January^{19,28,63,64}. This influences the seasonal frequency of the synoptic weather patterns that favour the connection between East Antarctica and Southeast Australia. SOM3 (elevated fire weather and decreased sea-salt concentrations), is more likely to occur in weakened polar vortex years ($r_{\text{Spearman}} = +0.65$, $p < 0.01$), early vortex breakdown years ($r_{\text{Spearman}} = -0.61$, $p < 0.01$) and negative SAM conditions (ONDJ $r_{\text{Spearman}} = -0.76$, $p < 0.01$). Conversely, SOM7 (reduced fire weather and increased sea-salt concentrations), is more likely to occur in strengthened polar vortex years ($r_{\text{Spearman}} = -0.45$, $p < 0.01$), late vortex breakdown years ($r_{\text{Spearman}} = +0.53$, $p < 0.01$) and positive asymmetric SAM conditions (ONDJ $r_{\text{Spearman}} = +0.54$, $p < 0.01$) (Fig. 3a, b; Supplementary Table 1). The influence of the polar vortex conditions on the seasonal persistence and frequency of SOM3 and SOM7 helps to connect the

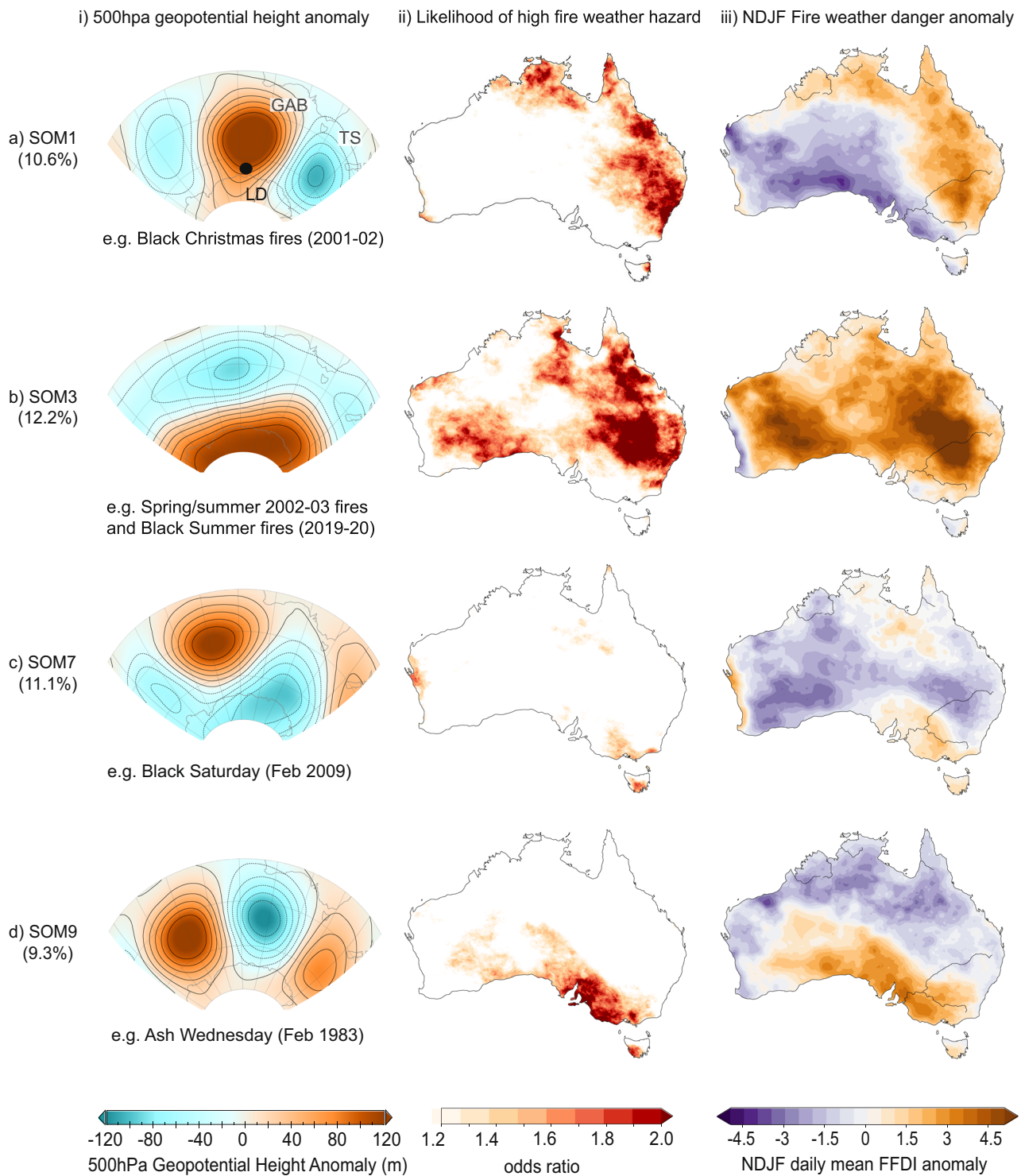


Fig. 2 | Southern Ocean synoptic weather conditions associated with elevated fire weather hazard over southeast Australia. Mean NDJF frequency of SOM nodes (defined in Udy et al.⁴⁶) over 1979-2018 in brackets - e.g. SOM1 (10.6%) (i) 500hpa geopotential height anomalies of SOM nodes associated with elevated fire weather over southeast Australia (data: ERA-Interim). Positive height anomalies are shown in red with solid contours and represent regions of anticyclonic ridging into mid-high latitudes. Negative height anomalies are shown in blue with dotted contours and represent regions of low pressure extending further north than usual. Example

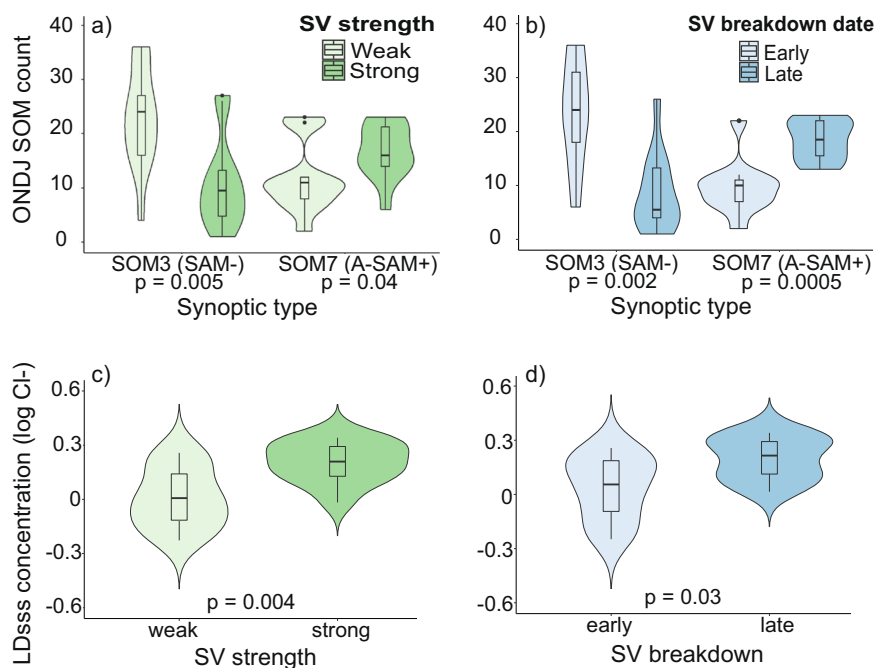
fire disasters associated with synoptic conditions listed. LD = Law Dome ice core location, GAB = Great Australian Bight, TS = Tasman Sea. (ii) Changes in the likelihood of high fire danger days (FFDI > 90th percentile 1951–2016) during the occurrence of each SOM node. *p*-value < 0.05 was used for significance and non-significant results were blank. (iii) Seasonal (November - February) daily FFDI anomaly for each SOM node. Refer to Supplementary material for odds ratio (Supplementary Fig. 5) and FFDI anomaly (Supplementary Fig. 6) composites for the remaining SOM nodes.

daily synoptic-scale conditions to the seasonal signal preserved in the Law Dome ice core record, and the connection to seasonal fire weather, rainfall, temperature, and vapour pressure deficit conditions over Australia (Supplementary Fig. 2).

The strength and seasonal breakdown timing of the stratospheric polar vortex explains 18% (*p* < 0.005) and 15% (*p* < 0.01) of the variability in the Law Dome sea-salt aerosol record respectively, with weakened vortex / early seasonal breakdown years characterised by decreased sea-salt aerosol

Fig. 3 | Synoptic type frequency and Law Dome summer sea-salt concentration during weakened/early breakdown and strengthened/late breakdown Antarctic stratospheric vortex conditions.

a October–January (ONDJ) synoptic type (Udy et al.⁴⁶) frequency during weak (S–T mode > 0.48, $n = 13$) and strong (S–T mode < -0.73, $n = 12$) vortex conditions using S–T mode (Lim et al.⁶⁴) to define vortex strength and coupling to the troposphere (positive values = weakened vortex conditions in S–T mode). SOM3 is associated with negative SAM (SAM-) conditions. SOM7 is associated with asymmetric positive SAM (A-SAM+) conditions (refer to Supplementary Table 1). **b** ONDJ synoptic type frequency during early (<27th November, $n = 12$) and late (>11th December, $n = 13$) stratospheric vortex breakdown date (Black & McDaniel⁶³; average breakdown = 4th December). **c** LDsss concentration during weak/strong vortex years. **d** LDsss concentration during early/late stratospheric vortex breakdown years. The Wilcoxon Signed Rank Test was used to test if there was a significant difference (95%) between the mean LDsss concentration or mean frequency of synoptic types during weakened/early breakdown and strengthened/late breakdown stratospheric vortex conditions.



concentrations in snowfall at Law Dome (Supplementary Table 1). The mean sea-salt aerosol concentration between weak and strong, or early and late, seasonal breakdown stratospheric vortex conditions are also significantly different (Fig. 3c, d). The strongest signal is observed in strengthened vortex years due to more consistent sea-salt aerosol concentration signals in the three synoptic types linked to increased sea-salt concentrations in snowfall at Law Dome⁵⁴.

2000-year reconstruction of summer fire weather hazard for southeast Australia

The Law Dome summer sea-salt (LDsss) aerosol concentration record was used to reconstruct Common Era area average summer (November to February) fire weather hazard over an eastern sector of southeast Australia (Figs. 4, 5). The selected reconstruction region reflects the confluence of the area of southeast Australia where the ice core record is strongly related to fire weather (Fig. 1c) and the forested coastal and alpine regions that were severely impacted by the Black Summer fires (Fig. 5g). The reconstruction was calculated using a linear regression model with 95% prediction intervals. The linear model was calibrated over the 1960–1990 period and validated over 1994–2016 period. The years influenced by the Pinatubo eruption (1991, 1992 & 1993) were excluded from the calibration and validation periods (Methods). The reconstruction reasonably captures both the observed year-to-year and decadal variability of above-average fire weather between 1951–2016 ($r = 0.4$ $p < 0.001$, RMSE = 2.2) (Fig. 4a, b; Supplementary Table 2). It is important to note that the mean reconstruction underestimates magnitude and does not capture all variability in fire weather in southeast Australia. However, most observations (>95%) are within the 95% prediction interval and the reconstruction performs better than climatology over the overlap period with observations (1951–2016) (Supplementary Fig. 3, Supplementary Table 2). Prior to the FFDI observational period, periods of increased fire activity reported in historical records⁶⁵ align with elevated fire weather conditions in the LDsss reconstruction, including large fires in the late 1920s and 1930s (Fig. 4a). The synoptic connection between East Antarctica and Australia provides insight into the type of fire weather synoptic-scale conditions that our reconstruction is sensitive to (i.e. SOM3, SOM7) (Fig. 4c, d), as well as the conditions likely missed by our reconstruction (i.e. SOM1, SOM9).

Our reconstruction suggests that the November to February seasonal average fire weather magnitude of the 2019/20 ‘Black Summer’ season was

likely extremely rare over the past 2000-years (Fig. 5a). The long-term climatological average (represented by 30 yr loess filter) indicates that the fire weather magnitude of the Black Summer and preceding seasons was outside the range of both observed and pre-industrial experience, crossing the $+2\sigma$ of the 1850–1900 reconstruction mean (Fig. 5a). The observed 2019/20 FFDI magnitude (15.1) was exceeded seven times (chronological order: 485, 683, 709, 760, 862, 885, 1108 CE) in the reconstruction when the upper estimate of the 95% prediction interval is considered. However, the long-term reconstructed climatological average during all these previous elevated fire weather seasons remained below the $+2\sigma$ of the 1850–1900 reconstruction mean. The reconstruction also indicates that the latest increase in fire weather commenced around 1850 CE, aligning with the beginning of the rapid rise in anthropogenic greenhouse gas concentrations⁶⁶. The indication of increased fire weather from 1850 CE is also reflected in charcoal records from sediment cores across southeast Australia⁶⁷.

The observed increased frequency of above-average fire weather conditions in southeast Australia^{3,14,16} is evident in the decade preceding the 2019/20 fires with 8 of the 11 years in the 2010–2020 period experiencing seasonal fire weather conditions exceeding the 1960–1990 average (Fig. 4b). Over the past 2000-years, this level of elevated fire weather hazard at a decadal timescale has been extremely rare, with one equivalent cluster in the observational record (1980s) and six clusters prior to observations (486–496, 1173–1176, 1193–1195, 1229–1231, 1233–1234, 1243–1247) (Fig. 5b). Both the elevated fire weather magnitude and increased decadal frequency clusters indicated by the 2000-year reconstruction occur prior to 1250 CE, which is beyond the period covered in existing seasonal rainfall⁴⁰ and drought⁶⁸ reconstructions for southeast Australia (Fig. 5e, f).

The reconstructed period of elevated fire weather magnitude and frequency at 485 CE and increased frequency of above average fire weather between 1150–1250 CE align with negative SAM conditions in multi-proxy reconstructions^{69,70} which is a key feature associated with increased drought, elevated maximum temperatures, and fire weather activity over southeast Australia^{3,14,23,71–73}. The significant relationships between the Law Dome record, FFDI, maximum temperature, and rainfall are also consistent with the austral spring–summer influence of negative SAM conditions on elevated fire weather (Supplementary Figs. 2, 3a).

The elevated fire weather conditions prior to 1250 CE indicated by the LDsss reconstruction are also consistent with periods of elevated maximum

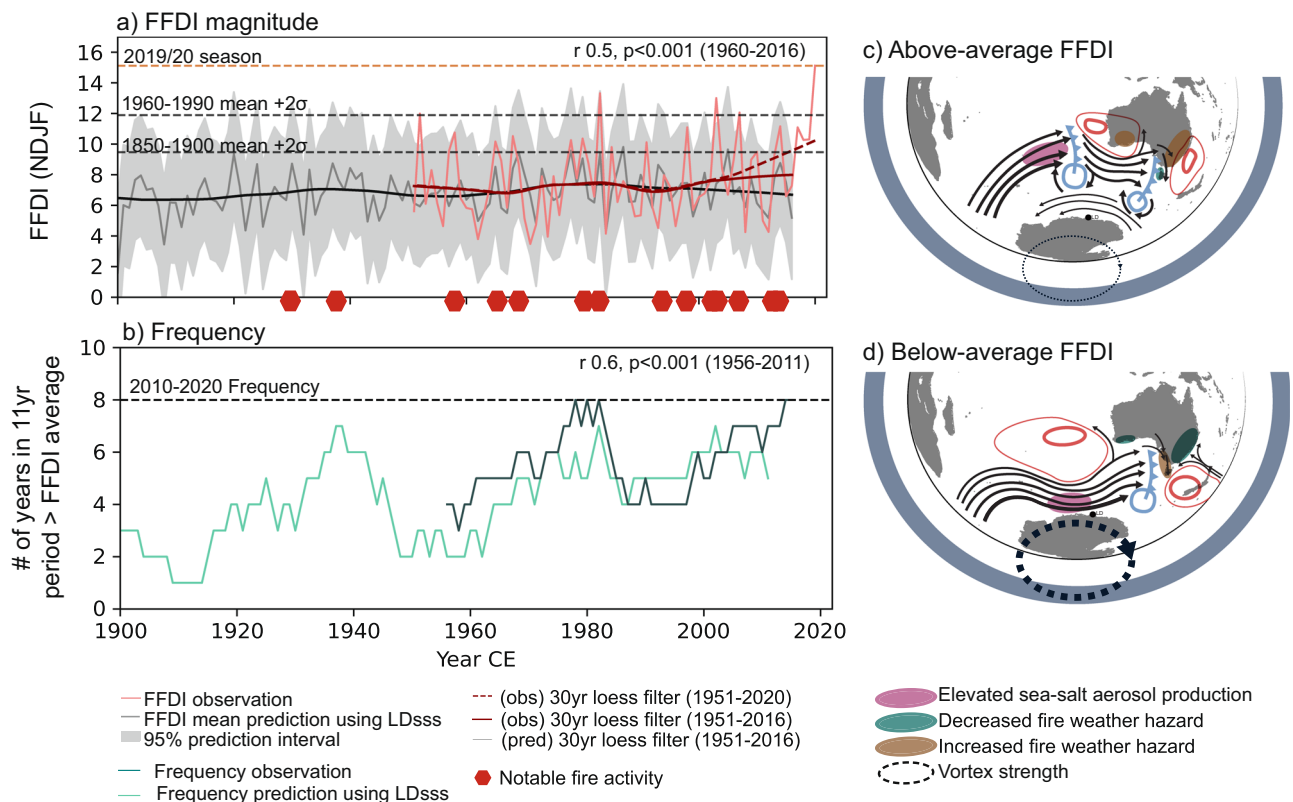


Fig. 4 | Southeast Australia fire weather magnitude and frequency variability from 1900-2020 and synoptic conditions the reconstruction is sensitive too.
a Late austral spring-summer (November to February) observed FFDI (Dowdy et al.²⁸) and FFDI prediction (this study) over the forested east coast and alpine regions of southeast Australia using the LDSS record (refer to the hatched area in Fig. 5g for reconstruction region). Light grey shading represents 95% prediction interval of the FFDI mean reconstruction. The long-term signal is represented as a 30-year loess filter of the NDJF seasonal mean for observations (dark red; the dashed line includes data to the 2019/20 season, the solid line includes data to 2015/16 season) and LDSS prediction (black). The observed 1960–1990 mean +2σ and predicted 1850-1900 mean +2σ are shown. Note the 1960-1990 FFDI mean (7.13) is equal between the observations and prediction. Red hexagons = notable fire activity reported within or near the reconstruction region (area burned >0.5 M ha and/or properties/lives lost - 1926/27; 1938/39;

1957/58; 1964/65; 1968/69; 1979/80; 1982/83; 1993/94; 1997/98; 2001/02; 2002/03; 2006/07; 2012/13; 2013/14) (see Methods). **b** Number of 11-year moving periods with November to February seasonal FFDI observations and prediction > 1960–1990 mean (7.13). **c** Schematic of surface synoptic-scale weather systems (black solid arrows represent wind direction, red lines indicate the location of high-pressure systems, blue lines indicate low pressure/cold fronts) and stratospheric Antarctic polar vortex conditions (strength indicated by width of dashed arrows) over November to February that support the connection between above average fire weather hazard in eastern Australia and decreased Law Dome summer sea-salt aerosol concentration in the East Antarctic ice core. **d** As for c, favourable conditions for supporting the connection between below-average fire weather hazard in eastern Australia and increased Law Dome summer sea-salt aerosol concentration. Location of Law Dome marked with black dot.

temperature and charcoal accumulation in lower-temporal resolution reconstructions from speleothems and lake sediment records within our FFDI reconstruction area (Fig. 5). The speleothem reconstruction from Yarrangobilly Caves⁴³ supports increased temperature during times of decreased sea-salt aerosol concentrations in the Law Dome record (Supplementary Fig. 2a) and increased reconstructed fire weather, with periods of elevated maximum temperatures consistent with 2000CE levels between ~500–800CE (Fig. 5c). A nearby alpine lake sediment record (Club Lake)⁴⁴ also indicates increased maximum temperature and elevated fire activity around ~500–900CE (Fig. 5c, d).

Implications for quantifying changing fire hazard frequency

Observational records, as well as palaeoclimate records extending only over recent centuries, underestimate the range of possible natural variability in elevated fire weather hazard frequency over southeast Australia. Previous periods with elevated fire weather hazard frequency, consistent with the decade preceding the Black Summer, all occurred prior to 1250CE. This suggests that the existing annually resolved rainfall and drought reconstructions^{40,68} in southeast Australia that cover the past ~500 years likely underestimate the possible natural variability of rainfall and temperature, and their contribution to fire weather over the Common Era (Fig. 5). The LDSS fire weather prediction indicates consistent average fire

hazard between the full Common Era prior to the 20th century (FFDI average = 6.4) and the pre-industrial baseline used by the Intergovernmental Panel on Climate Change (1850-1900CE; FFDI average = 6.7). However, the 30-year loess filter indicates that within the Common Era there are six extended periods (mid-year points; 290CE, 490CE, 900CE, 1000CE, 1200CE and 1720CE) with naturally elevated fire weather beyond the pre-industrial baseline that is important to consider alongside anthropogenic forcing. Local rainfall, temperature, and drought severity reconstructions also indicate relatively (compared to 1850-1900 baseline) warmer and drier conditions around 1200CE^{43,74} and early 1700s^{40,68} (Fig. 5). Using the 1850–1900CE baseline period for contextualising present day climate change could underestimate the total possible fire weather hazard when the anthropogenically forced trend in fire weather is combined with the full range of possible natural variability evident over the Common Era.

Conclusions

Our reconstruction highlights the rarity of extended periods of elevated fire weather hazard within a natural climate variability context and the importance to plan for more intense and frequent fire weather beyond what has been recorded in the observational record. We show that the intensity of the 2019/20 Black Summer fire weather was unprecedented since observations began in 1950, but there are seven analogue periods of similar

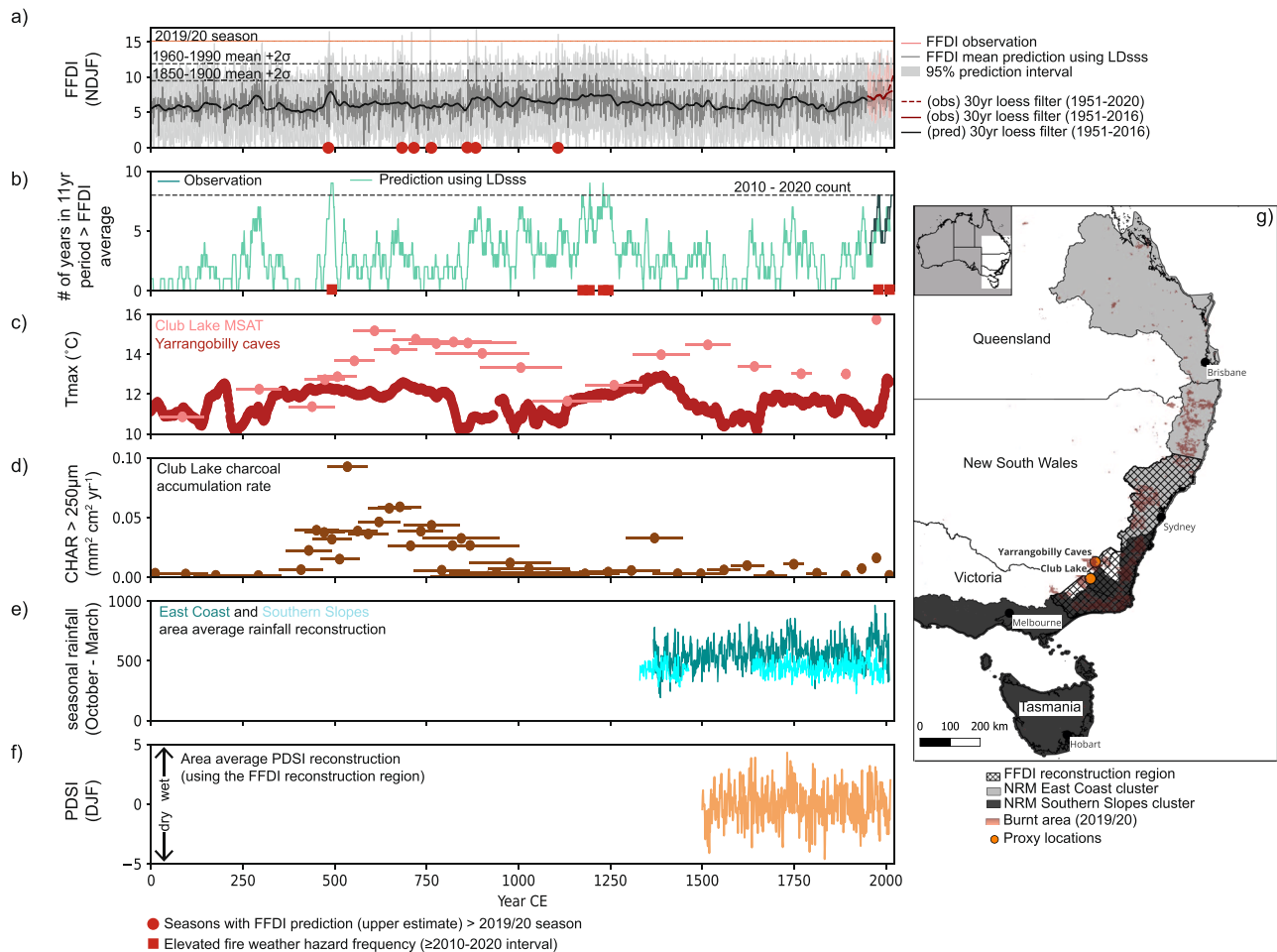


Fig. 5 | Fire weather reconstruction from the Law Dome summer sea salt (LDss) aerosol concentration record compared to local palaeoclimate records.

a Observed FFDI (Dowdy et al.²⁸) and 2000+ year (1-2016 CE) FFDI mean reconstruction over the forested east coast and alpine regions of southeast Australia using the LDss record (hatched area in map inset (g)). Light grey shading represents 95% prediction interval of the FFDI mean reconstruction. The long-term signal is represented as a 30-year loess filter of the NDJF seasonal mean for observations (dark red); the dashed line includes data to the 2019/20 season, the solid line includes data to 2015/16 season) and FFDI mean prediction using LDss (black). Red circles indicate potential analogue seasons where the upper estimate (95% prediction interval) of the reconstruction exceeded the observed FFDI over the 2019/20 season. **b** Number of seasons over an 11-year period with NDJF seasonal FFDI observations and

prediction > 1960-1990 mean (7.13). Red squares indicate potential analogue periods of increased decadal frequency of above-average fire weather. **c** Reconstructed maximum temperature from Yarrangobilly Caves (McGowan et al.⁴⁴) and mean summer temperature from Club Lake (Thomas et al.⁴⁵). Approximate age model dating error for Club Lake indicated by horizontal lines. **d** Charcoal (>250 µm) accumulation rate from Club Lake (Thomas et al.⁴⁵). Approximate age model dating error indicated by horizontal lines. **e** Warm season (October–March) rainfall reconstruction for East Coast and Southern Slopes NRM regions (Freund et al.⁴¹). **f** Austral summer (DJF) Palmer Drought Severity Index (PDSI) area average reconstruction (Palmer et al.⁶⁸) over the FFDI reconstruction region. **g** Map of eastern Australia including the FFDI reconstruction area, 2019/20 burnt area, local proxy records, and NRM rainfall reconstruction regions.

extreme fire danger caused by natural variability in the 2000-year reconstruction. Additionally, the frequency of above-average fire weather in the period leading up to and including the Black Summer (2010-2020) has only occurred once since 1950 (early 1980s) and six times in the reconstruction. Previous elevated fire weather hazard periods, such as the 485–495CE period, could provide analogues for understanding fire weather variability under a warmer and drier background climate. Nine years (out of 11) during this period were estimated to have experienced above average (1960–1990) fire weather hazard, with the mean reconstructed FFDI magnitude in 485CE above the 1960–1990 mean + 2σ threshold, and the peak reconstructed value (upper estimate) exceeding the 2019/20 season (Fig. 5a). With atmospheric carbon dioxide concentration relatively stable during this period⁶⁶, the elevated fire weather hazard and associated drier conditions and warmer temperatures across southeast Australia indicated by both local and remote palaeoclimate proxies demonstrate the extremes in fire weather that are possible from natural climate variability alone.

While intervals of the Common Era provide examples of increased fire weather magnitude and frequency in southeast Australia, the climate change

signal that is now driving the increase in fire weather is unprecedented over the last two millennia (Fig. 5a). The climate change signal, as indicated by a 30-year loess filter of the seasonal FFDI, has moved outside of the historical experience based on the reconstructed 1850–1900 preindustrial reference period and is approaching the bounds of historical experience based on the observed 1960–1990 reference period. At no other time during the last two millennia of reconstruction did long-term changes in the FFDI state exceed these thresholds. The extended perspective on the natural variability of fire weather, indicated by the annually resolved Law Dome summer sea-salt reconstruction, is important to consider in wildfire hazard planning, on top of the recent observed and predicted increases in frequency, duration, and intensity of fire weather in southeast Australia associated with anthropogenic warming^{25,38,75,76}.

Methods

Law Dome summertime sea-salt concentration record

The Law Dome summertime sea-salt (LDss) aerosol concentration record^{51,77} was used to reconstruct southeast Australian fire weather. The ice

core site (Dome Summit South: DSS) receives a high annual snowfall of 0.69 metres of ice equivalent/year (~1.5 m of snowfall)^{51,78} which produces seasonally varying annual layers in the ice core and corresponds to annual and seasonal climate signals^{53,79,80}. The DSS composite record used in this study is comprised of four overlapping ice cores; DSS1617 (1990–2016), DSS97(1888–1989), DSS99 (1841–1887), and DSS Main (1841–0)⁵¹. The DSS ice core record was dated using seasonally varying water stable isotopes ($\delta^{18}\text{O}$ and δD) which peak in austral summer (early January average) combined with confirmatory analysis of seasonally varying trace chemistry species⁵¹. These annually resolved and accurately dated layers⁵⁰ make the Law Dome record useful for hydroclimate studies where accurate event timing, duration and high sample temporal resolution (seasonal–annual) are required⁸¹. Over the Common Era, a conservative estimate of dating error is zero between 2016–1815CE (Tambora eruption), then a maximum of +1 year between 1815–1257CE (Samalala eruption), and a maximum of +6/–11 years between 1257–422CE⁸².

The LDSS record is derived from trace chemical analysis via ion chromatography of discrete samples ranging from 2.5 cm to 5 cm resolution over the 2000-year record⁸². The sample resolution between 1300–2016 CE was 5 cm. This equates to an average sample resolution of 21 samples/year for the period 1950–2016CE and 12 samples/year for the period 1300–1950CE. To contend with the thinning of annual layers with depth, the sample resolution was increased to 3 cm from 980–1300 CE and 2.5 cm between 10 BCE–980 CE (equates to an average of 8–11 samples per year for the 10BCE–1300 CE). The mean annual sample resolution over the 2000-year record is ~10 samples per year⁸². Assuming seasonally uniform snowfall, the chloride record is split into 12 estimated monthly snowfall accumulation bins, based on the estimated snowfall accumulation for each year derived from the annual layer horizons. The LDSS record is then calculated by averaging the sea-salt chloride concentration for December to March (DJFM) period chloride log transformed⁵³ concentrations (Supplementary Fig. 7). The split between December and January in the ice core record is determined by the placement of the annual horizon which is informed by the summer water stable isotope peak and seasonally varying trace chemistry. While Law Dome receives frequent snowfall, the accumulation is not completely uniform⁵⁴. Thus, the ice core 'DJFM' period approximates the austral summer period but does not directly align with DJFM atmospheric conditions. Udy et al.⁵⁴ observed the strongest connection to atmospheric conditions from November to February (NDJF). To develop the 2000-year record, at least two out of the four bins in the 'DJFM' ice core period were required to calculate a DJFM mean concentration. If less than two bins over the DJFM period contained data (i.e. sample gap from missing ice core material), the 'DJFM' year was removed from the record. Refer to Vance et al.⁸² for more details on the development of the LDSS record.

Synoptic typing dataset. The daily synoptic typing dataset for the southern Indian Ocean^{47,83}, was used to classify the dominant large-scale weather patterns of each day from January 1979 to October 2018. This dataset was created using a self-organising maps algorithm on 500hPa geopotential height daily anomalies from ERA-Interim reanalysis data⁵⁸. The synoptic typing dataset consists of nine key synoptic-scale weather patterns over the southern Indian Ocean, ranging from zonal to meridional anomalies⁴⁷. Refer to Udy et al.^{47,54} for more detail.

Quantifying historical fire weather conditions. The daily Australian McArthur Forest Fire Danger Index (FFDI)^{27,84} is used to represent the influence of surface weather conditions on fire weather hazards over Australia, and is based on daily maximum temperature, relative humidity, wind speed, and recent rainfall⁸⁴. Here we quantify the relationship between the Law Dome summer sea-salt (LDSS) aerosol concentration record⁵¹ and fire-promoting weather and climate conditions across Australia based on the FFDI²⁷. Increased FFDI values represent an increase in the likelihood of fire activity in the region if fuels and ignition sources are available, with hotter, drier, and windier conditions priming vegetation to

burn. The FFDI values used in this study are based on the calculations and datasets described in Dowdy (2018)²⁷ and is calculated as:

$$FFDI = \exp^{0.0338T - 0.0345RH + 0.0234v + 0.243147} \times DF^{0.987}$$

where T is the daily maximum surface air temperature (°C), RH is relative humidity (%), v is wind speed (km/h) and DF is the drought factor. The input variables used in Dowdy (2018)²⁷ FFDI calculations consist of a gridded analysis of observations from the Australian Water Availability Project (AWAP)⁸⁵ for daily maximum temperature, daily accumulated rainfall (24 hr period to 09:00 local time each day) and vapor pressure at 15:00 local time. The vapor pressure observations were used to calculate the relative humidity at the approximate time of maximum temperature. The 6-hourly NCEP-NCAR reanalysis data⁸⁶ were used for surface winds at 06:00 UTC to represent mid-afternoon wind speed over Australia.

The drought factor estimates the availability of fuel to burn by combining soil moisture deficits (representing seasonal dryness) and recent rainfall (past 20 days). The Keetch-Bryam Drought Index (KBDI) is a simplified water balance model and estimates daily soil moisture deficit based on the soil moisture deficit of the previous day, effective precipitation (amount of precipitation infiltrating the soil), and evapotranspiration (derived from the previous days soil moisture deficit, maximum temperature and mean annual rainfall to account for vegetation cover)⁸⁷.

The daily Australian Gridded Climate Data (AGCD) v1 maximum temperature and rainfall data⁸⁸, KBDI²⁷, and ERA5 2 m temperature and relative humidity⁸⁹ are used to investigate the relationship between LDSS and the surface weather components of the FFDI calculation and vapour pressure deficit (atmospheric aridity; calculated for each grid point using ERA5 2 m temperature and relative humidity as inputs into the Nolan et al.⁹⁰ equation). Daily datasets were aggregated to monthly and seasonal totals (for rainfall, count of synoptic types, and count of high fire danger days above 90th percentile) and averages (for FFDI, maximum temperature, KBDI, and vapour pressure deficit). Despite the obvious relationship between wind speed and fire weather, we excluded wind speed from our analysis because variability in fire weather over timescales longer than weekly is primarily driven by temperature, relative humidity, recent rainfall, and drought conditions²⁷. Monthly and seasonal wind speeds (in contrast to daily or hourly extremes) are unlikely to force increased fire hazards compared to the higher frequency winds associated with the passing of a cold front³⁰. Instead, monthly or seasonal wind speed conditions are more likely to reflect the intensification or reduction in the surface easterly winds over austral spring and summer^{60,91}.

Synoptic-weather scale connection and Antarctic stratospheric polar vortex influence. The potential climate dynamics driving the relationship between the LDSS record and Australian climate were investigated using a synoptic weather typing dataset for the southern Indian Ocean^{47,54} and indices representing the strength⁶⁴ and seasonal breakdown timing anomaly⁶³ of the Antarctic stratospheric polar vortex. Spearman correlation and linear regression analysis between the LDSS record, synoptic type frequency, and stratospheric vortex indices were performed between 1979–80 to 2015–16 over the October to January (ONDJ) period as the coupling between the Antarctic stratospheric vortex and tropospheric circulation is strongest over this period⁶⁴. All time series were detrended to remove linear trends and tested for autocorrelation and normality (Shapiro Wilkes test). No significant autocorrelation (lag-1) was detected. Spearman correlation was used to account for some synoptic type frequency time series not being normally distributed. The two-sided Student's *t*-test was used to test the significance (95%) of the observed correlation score.

The stratospheric vortex strength⁶⁴ and breakdown timing anomaly⁶³ datasets were also split into upper (>66%, $n = 13$) and lower (<33%, $n = 12$) tercile years for the period 1979–2016 to explore frequency distribution and mean changes in LDSS concentration and synoptic type frequency between weak/early and strong/late stratospheric vortex conditions. The Wilcox

Signed Rank Test was used to determine if the mean difference between the upper and lower tercile groups was statistically significant at the 95% level. The middle tercile group was not assessed.

Correlation between FFDI, LDss, and large-scale modes of climate variability. Pearson correlation analysis on detrended time series was performed between the LDss record, FFDI, and related climate variables at each grid point across Australia over the late Austral spring-summer season (November to February; NDJF). These results were compared to the strength and spatial pattern of the relationships between SAM (using the Marshall index⁹²) and ENSO (using the Southern Oscillation Index⁹³) with the FFDI²⁷ over NDJF. Two time periods (1950–51 to 2015–16 and 1979–80 to 2015–16) were selected to account for different dataset lengths. Significance was tested using a two-sided Student's *t* test for $p < 0.05$. The false discovery rate⁹⁴ was also determined for the spatial correlation between LDss and FFDI as equivalent to $p < 0.01$.

Regional average FFDI was also calculated over the forested coastal and alpine region of southeast Australia which includes southeast New South Wales (including Australian Capital Territory) and Northeast Victoria (Fig. 5g) and correlated with LDss. This region is mostly east of the Great Dividing Range, and was heavily impacted by the 2019/20 Black Summer Fires.

Odds ratio of high fire danger days occurring in low vs non-low aerosol sea-salt concentration conditions. To determine the probability of a high fire danger day (FFDI > 90th percentile 1950/51 to 2015/16) under different ice core sea-salt aerosol concentration conditions and synoptic type occurrence, the number of days between November and February with FFDI >90th percentile was calculated for each NDJF season (using the FFDI gridded dataset).

A LDss concentration threshold of $0.05 \mu \text{Eq L}^{-1}$ (LDss lower tercile 1950–2016) was used to classify low ($<0.05 \mu \text{Eq L}^{-1}$) and non-low ($\geq 0.05 \mu \text{Eq L}^{-1}$) sea-salt concentration seasons. An odds ratio was used to test the ratio of the probability of occurrence of high fire danger days (count/season) between low (22 years) and non-low (45 years) sea-salt years in the ice core dataset. The null hypothesis was that there was no significant difference in the number of high fire danger days between the two groups, and the odds ratio would be 1. The null hypothesis was rejected if the odds ratio was greater than 1.2 ($p < 0.05$) using the Fisher exact test.

The changes in the likelihood of high fire danger days occurring during each synoptic type were also tested using odds ratio and the Fisher exact test for significance ($p < 0.05$). For each synoptic type, the number of high fire danger days within each NDJF season occurring on days classified as SOMx (y^1) vs the number of high fire danger days on other days (y^2) was tested using the following equation:

$$\text{Odds ratio SOMx} = \frac{y^1(\text{no. high fire danger days on SOMx})/z^1(\text{no. of non high fire danger days on SOMx})}{y^2(\text{no. high fire danger days on non SOMx})/z^2(\text{no. of non high fire danger days on non SOMx})}$$

Fire weather hazard reconstruction. The LDss record (predictor variable) was used to reconstruct area average seasonal (NDJF) FFDI over eastern Australia (Fig. 5g). This region incorporates the coastal and alpine regions of southeast Australia that were severely impacted by the 2019–20 Black Summer fires. The fire season for this region is generally between October to March²⁷. A linear regression model was trained over the 1960–1990 period and validated over 1994–2016. Observational data between 1950–1959 were excluded from the model training period due to uncertainty in the input data used to calculate the FFDI during this period (e.g. number of available weather stations used in the rainfall and temperature gridded datasets increase by >20% in the late 1950s)⁸⁵. Additionally, the 1950's were an unusually wet period across eastern Australia due to high frequency of East Coast Low systems and multiple La Niña events^{95,96}. The sensitivity of the results to excluding 1950–1959 from the training period was tested by comparing the 2000-year prediction results from the two periods; 1960/61–1989/90 (model1: $r^2 = 0.4$, $p < 0.0001$) and 1950/51 – 1989/90

(model2: $r^2 = 0.22$, $p < 0.002$). The difference between the 2000-year prediction from the two prediction models was minimal (model1: mean FFDI = 6.2, sd = 1.6; model 2: mean FFDI = 6.5, sd = 1.3) (Supplementary Fig. 7). Importantly, the number of elevated fire weather seasons in both reconstructions that met or exceeded the 2019/20 magnitude (considering the 95% prediction interval) were consistent. The years influenced by the Pinatubo eruption (1991,1992 & 1993) were also excluded from the calibration and validation periods due to the impact of stratospheric sulfate aerosols on regional climate⁹⁷. Sulphuric acid related to volcanic activity also reacts with the chloride component of sea-salt in both the atmosphere and the firm which can temporarily disrupt the deposition and preservation of the chloride sea-salt concentration in the ice core records^{98,99}.

The predict function in R with the trained linear model and the 95% prediction interval was used to calculate the 2000-year reconstruction using the LDss values. The prediction interval reflects the prediction uncertainty around a single value in the reconstruction. All observed FFDI values in the calibration period (1960–1990) are within the 95% prediction interval. In the validation period (1994–2016), the observed FFDI values are within the 95% prediction interval for 21 of the 23 seasons. Two elevated fire weather seasons in the validation period (2002/03, 2006/07) are underestimated by reconstruction uncertainty (i.e. the upper prediction interval is less than the observed FFDI) (Supplementary Fig. 3).

The model fit was assessed by comparing the mean reconstruction and observations for the calibration, validation, 1960–2016 and 1951–2016 periods using Pearson and Spearman correlation score (*r*), adjusted r^2 , root mean square error (RMSE) and Nash-Sutcliffe model efficiency coefficient (NSE) (Supplementary Table 2). RMSE is an absolute measure of the fit representing the variance of the model errors, with smaller values indicating a better fit. An NSE value greater than 0 indicates the reconstruction performs better than the climatology of the reconstructed period¹⁰⁰.

The area average FFDI mean reconstruction was used to determine above/below 1960–1990 FFDI average (FFDI = 7.13) conditions. The average FFDI over 1960–1990 was consistent between observations and reconstruction. The accuracy of predicting above/below average FFDI conditions was tested using a logistic regression model. An 11 yr running count of above-average seasons was used to identify decadal periods with elevated fire hazard over the 2000-year reconstruction.

The LDss record currently only extends to the 2015/16 season so cannot be directly compared to the 2019/20 Black Summer season. Based on the synoptic weather conditions (i.e. frequent cold fronts), persistent and record negative SAM conditions, and weakened Antarctic stratospheric polar vortex observed over the 2019/20 fire season^{19,31} we expect the summer sea-salt aerosol concentration in the next Law Dome update to be very low.

Time of emergence. The emergence of signals of long-term change was assessed using observed and predicted FFDI. We used a 30-year loess filter to calculate a moving long-term climatological value¹⁴ over the 2000-year reconstruction and observed datasets, and compared the moving window value to the variability (2σ) within two reference periods; 1960–1990 (observed) and 1850–1900 (reconstruction). The observed filter was calculated over 1951–2016 and 1951–2020 to account for the overlap period with the ice core record that was only available to 2016.

Between 1951–2016, the reconstructed 30-year climatology has minimal error (average difference 0.33/4% of observed value) but does underestimate the observed climatology (difference > 0.8/>10% of observed value) between 1951–1954 and 2006–2016.

Comparison to historical records and local palaeoclimate records. Prior to FFDI observations beginning in 1950, we compared the LDss FFDI mean reconstruction with historical records of major documented fire events (e.g. Bushfire inquiry documents⁶⁵), local archives that extended back 2000-years within the reconstruction region (Club Lake⁴⁴ and Yarrangobilly Caves⁴³) and multi-proxy palaeoclimate reconstructions (warm season rainfall for eastern and southeast Australia⁴⁰ and the Palmer Drought Severity Index⁶⁸) (Fig. 5g).

We also identify notable fire activity (area burnt >0.5 M ha and/or reports of property/lives lost) since 1900 based on synthesised information available from Abram et al.¹⁴; Canadell et al.¹⁶, National Inquiry on Bushfire Mitigation and Management⁶⁵, NSW parliamentary analysis¹⁰¹ and a UNSW fire history storyboard (<https://100-years-of-bushfire-unsu-au.opendata.arcgis.com/>).

Data availability

The 2000-year FFDI reconstruction (FFDI mean magnitude and 11-year frequency of above-average conditions) calculated in this study is available through the Australian Antarctic Data Centre - <https://doi.org/10.26179/bjfa-rd82>. Other datasets used in this study are available online in the following locations: ERA5: <https://cds.climate.copernicus.eu/cdsapp#!/dataset/reanalysis-era5-single-levels?tab=overview>. The daily synoptic typing dataset for the southern Indian Ocean from 1979–2018: https://data.aad.gov.au/metadata/records/AAS_4537_z500_SynopticTyping_SouthernIndianOcean, and the Law Dome summer sea-salt record from https://data.aad.gov.au/metadata/records/DSS_2k_data_compilation. The Marshall station index, representing the Southern Annular Mode: <https://legacy.bas.ac.uk/met/gjima/sam.html>. The Southern Oscillation Index used to represent El Niño–Southern Oscillation is available from the Australian Bureau of Meteorology - SOI: <http://www.bom.gov.au/climate/enso/soi/>. The Australian Gridded Climate Data (AGCD) v1 is published by the Australian Bureau of Meteorology, and freely accessible to registered researchers here: <http://www.bom.gov.au/metadata/catalogue/19115/ANZCW0503900567>. FFDI and KBDI data were provided by Andrew Dowdy and accessible for research by contacting the Australian Bureau of Meteorology. The stratospheric vortex strength and breakdown timing anomaly datasets were provided by EunPa Lim and available on request by contacting the Australian Bureau of Meteorology. The palaeoclimate reconstructions included in Fig. 5 were accessed from: Yarrangobilly Caves - <https://espace.library.uq.edu.au/view/UQ:22d3d4d>; East Coast and Southern Slopes rainfall reconstruction - <https://doi.org/10.4225/49/59e3ee30cdbbc>; PDSI - <https://www.nci.noaa.gov/access/paleo-search/study/20245>. The Club Lake datasets were provided by Zoe Thomas and are available on request by contacting the corresponding author <https://doi.org/10.1016/j.scitotenv.2021.149542>.

Code availability

We used a combination of Python-v3 and R-v4.2.2 for our analysis. The code used for each figure is available through the corresponding author's github <https://doi.org/10.5281/zenodo.11147969>. https://github.com/dgudy91/SEAus_Fire_weather_2k_reconstruction.

Received: 18 October 2023; Accepted: 29 May 2024;

Published online: 13 June 2024

References

- Seneviratne, S. I. et al. Weather and climate extreme events in a changing climate. In *Climate Change 2021: The Physical Science Basis. Contribution of Working Group I to the Sixth Assessment Report of the Intergovernmental Panel on Climate Change* (eds Masson-Delmotte, V. et al.) pp. 1513–1766 (Cambridge University Press, New York, USA, 2021).
- Jones, M. W. et al. Global and regional trends and drivers of fire under climate change. *Rev. Geophys.* **60**, e2020RG000726 (2022).
- Richardson, D. et al. Increased extreme fire weather occurrence in southeast Australia and related atmospheric drivers. *Weather Clim. Extremes* **34**, 100397 (2021).
- Bowman, D. M. J. S. et al. Fire in the earth system. *Science* **324**, 481–484 (2009).
- Bowman, D. M. J. S. et al. Vegetation fires in the Anthropocene. *Nat. Rev. Earth Environ.* **1**, 500–515 (2020).
- Marlon, J. R. What the past can say about the present and future of fire. *Quat. Res.* **96**, 66–87 (2020).
- Jain, P., Castellanos-Acuna, D., Coogan, S. C. P., Abatzoglou, J. T. & Flannigan, M. D. Observed increases in extreme fire weather driven by atmospheric humidity and temperature. *Nat. Clim. Chang.* **12**, 63–70 (2022).
- de la Barrera, F., Barraza, F., Favier, P., Ruiz, V. & Quense, J. Megafires in Chile 2017: Monitoring multiscale environmental impacts of burned ecosystems. *Sci. Total Environ.* **637–638**, 1526–1536 (2018).
- Turco, M. et al. Climate drivers of the 2017 devastating fires in Portugal. *Sci. Rep.* **9**, 13886 (2019).
- Lagouvardos, K., Kotroni, V., Giannaros, T. M. & Dafis, S. Meteorological conditions conducive to the rapid spread of the deadly wildfire in Eastern Attica, Greece. *Bull. Am. Meteorol. Soc.* **100**, 2137–2145 (2019).
- Brown, T., Leach, S., Wachter, B. & Gardunio, B. The Extreme 2018 Northern California fire season. *Bull. Am. Meteorol. Soc.* **101**, S1–S4 (2020).
- Higuera, P. E. & Abatzoglou, J. T. Record-setting climate enabled the extraordinary 2020 fire season in the western United States. *Glob. Change Biol.* **27**, 1–2 (2021).
- Filkov, A. I., Ngo, T., Matthews, S., Telfer, S. & Penman, T. D. Impact of Australia's catastrophic 2019/20 bushfire season on communities and environment. Retrospective analysis and current trends. *J. Saf. Sci. Resil.* **1**, 44–56 (2020).
- Abram, N. J. et al. Connections of climate change and variability to large and extreme forest fires in southeast Australia. *Commun. Earth Environ.* **2**, 8 (2021).
- Zachariah, M. et al. Extreme Heat in North America, Europe and China in July 2023 Made Much More Likely by Climate Change. <http://spiral.imperial.ac.uk/handle/10044/1/105549> <https://doi.org/10.25561/105549> (2023).
- Canadell, J. G. et al. Multi-decadal increase of forest burned area in Australia is linked to climate change. *Nat. Commun.* **12**, 6921 (2021).
- Borchers Arriagada, N. et al. Unprecedented smoke-related health burden associated with the 2019–20 bushfires in eastern Australia. *Med J. Aust.* **213**, 282–283 (2020).
- Devanand, A. et al. Australia's Tinderbox Drought: An extreme natural event likely worsened by human-caused climate change. *Sci. Adv.* **10**, eadj3460 (2024).
- Lim, E.-P. et al. The 2019 Southern Hemisphere Stratospheric Polar Vortex weakening and its impacts. *Bull. Am. Meteorol. Soc.* **102**, E1150–E1171 (2021).
- van Oldenborgh, G. J. et al. Attribution of the Australian bushfire risk to anthropogenic climate change. *Nat. Hazards Earth Syst. Sci.* **21**, 941–960 (2021).
- Deb, P. et al. Causes of the Widespread 2019–2020 Australian Bushfire Season. *Earth's Future* **8**, e2020EF001671 (2020).
- Verdon, D. C. et al. Multi-decadal variability of forest fire risk—eastern Australia. *Int. J. Wildland Fire* **13**, 165–171 (2004).
- Harris, S. & Lucas, C. Understanding the variability of Australian fire weather between 1973 and 2017. *PLOS ONE* **14**, e0222328 (2019).
- Williamson, G. J. et al. Measurement of inter- and intra-annual variability of landscape fire activity at a continental scale: the Australian case. *Environ. Res. Lett.* **11**, 035003 (2016).
- Clarke, H., Lucas, C. & Smith, P. Changes in Australian fire weather between 1973 and 2010. *Int. J. Climatol.* **33**, 931–944 (2013).
- Sharples, J. J. et al. Natural hazards in Australia: extreme bushfire. *Clim. Change* **139**, 85–99 (2016).
- Dowdy, A. J. Climatological variability of fire weather in Australia. *J. Appl. Meteorol. Climatol.* **57**, 221–234 (2018).
- Lim, E.-P. et al. Australian hot and dry extremes induced by weakenings of the stratospheric polar vortex. *Nat. Geosci.* **12**, 896–901 (2019).
- Mariani, M., Fletcher, M.-S., Holz, A. & Nyman, P. ENSO controls interannual fire activity in southeast Australia. *Geophys. Res. Lett.* **43**, 10,891–10,900 (2016).

30. Fiddes, S. L., Pezza, A. B. & Renwick, J. Significant extra-tropical anomalies in the lead up to the Black Saturday fires. *Int. J. Climatol.* **36**, 1011–1018 (2016).
31. Cai, D., Abram, N. J., Sharples, J. J. & Perkins-Kirkpatrick, S. E. Increasing intensity and frequency of cold fronts contributed to Australia's 2019–2020 Black Summer fire disaster. *Environ. Res. Lett.* **17**, 094044 (2022).
32. Reeder, M. J. & Smith, R. K. A study of frontal dynamics with application to the Australian summertime “Cool Change”. *J. Atmos. Sci.* **44**, 687–705 (1987).
33. Mills, G. A re-examination of the synoptic and mesoscale meteorology of Ash Wednesday 1983. *Aust. Meteorol. Mag.* **54**, 35–55 (2005).
34. Mills, G. On the sub-synoptic scale meteorology of two extreme fire weather days during the Eastern Australian fires of January 2003. *Aust. Meteorol. Mag.* **54**, 907 (2005).
35. Dowdy, A. J., Fromm, M. D. & McCarthy, N. Pyrocumulonimbus lightning and fire ignition on Black Saturday in southeast Australia. *J. Geophys. Res.: Atmos.* **122**, 7342–7354 (2017).
36. Engel, C. B., Lane, T. P., Reeder, M. J. & Reznay, M. The meteorology of Black Saturday. *Q. J. R. Meteorol. Soc.* **139**, 585–599 (2013).
37. Clarke, H. et al. Forest fire threatens global carbon sinks and population centres under rising atmospheric water demand. *Nat. Commun.* **13**, 7161 (2022).
38. Abatzoglou, J. T., Williams, A. P. & Barbero, R. Global emergence of anthropogenic climate change in Fire Weather Indices. *Geophys. Res. Lett.* **46**, 326–336 (2019).
39. Richardson, D. et al. Global increase in wildfire potential from compound fire weather and drought. *npj Clim. Atmos. Sci.* **5**, 1–12 (2022).
40. Freund, M., Henley, B. J., Karoly, D. J., Allen, K. J. & Baker, P. J. Multi-century cool- and warm-season rainfall reconstructions for Australia's major climatic regions. *Climate* **13**, 1751–1770 (2017).
41. Croke, J. et al. A palaeoclimate proxy database for water security planning in Queensland Australia. *Sci. Data* **8**, 292 (2021).
42. Flack, A. L., Kiem, A. S., Vance, T. R., Tozer, C. R. & Roberts, J. L. Comparison of published palaeoclimate records suitable for reconstructing annual to sub-decadal hydroclimatic variability in eastern Australia: implications for water resource management and planning. *Hydrol. Earth Syst. Sci.* **24**, 5699–5712 (2020).
43. McGowan, H. et al. Global warming in the context of 2000 years of Australian alpine temperature and snow cover. *Sci. Rep.* **8**, 4394 (2018).
44. Thomas, Z. A. et al. Late Holocene climate anomaly concurrent with fire activity and ecosystem shifts in the eastern Australian Highlands. *Sci. Total Environ.* **802**, 149542 (2022).
45. Mariani, M. et al. Disruption of cultural burning promotes shrub encroachment and unprecedented wildfires. *Front. Ecol. Environ.* **20**, 292–300 (2022).
46. McMorrow, A., Van Ommen, T. D., Morgan, V. & Curran, M. A. J. Ultra-high-resolution seasonality of trace-ion species and oxygen isotope ratios in Antarctic firn over four annual cycles. *Ann. Glaciol.* **39**, 34–40 (2004).
47. Udy, D. G., Vance, T. R., Kiem, A. S., Holbrook, N. J. & Curran, M. A. J. Links between large-scale modes of climate variability and synoptic weather patterns in the Southern Indian Ocean. *J. Clim.* **34**, 883–899 (2021).
48. Morgan, V. I. et al. Site information and initial results from deep ice drilling on Law Dome, Antarctica. *J. Glaciol.* **43**, 3–10 (1997).
49. Souney, J. M. et al. A 700-year record of atmospheric circulation developed from the Law Dome ice core, East Antarctica. *J. Geophys. Res.* **107**, 4608 (2002).
50. Plummer, C. T. et al. An independently dated 2000-yr volcanic record from Law Dome, East Antarctica, including a new perspective on the dating of the 1450s CE eruption of Kuwae, Vanuatu. *Clim.* **8**, 1929–1940 (2012).
51. Jong, L. M. et al. 2000 years of annual ice core data from Law Dome, East Antarctica. *Earth Syst. Sci. Data* **14**, 3313–3328 (2022).
52. Pedro, J. B., Smith, A. M., Simon, K. J., van Ommen, T. D. & Curran, M. A. J. High-resolution records of the beryllium-10 solar activity proxy in ice from Law Dome, East Antarctica: measurement, reproducibility and principal trends. *Climate* **7**, 707–721 (2011).
53. Vance, T. R., van Ommen, T. D., Curran, M. A. J., Plummer, C. T. & Moy, A. D. A millennial proxy record of ENSO and Eastern Australian rainfall from the Law Dome Ice Core, East Antarctica. *J. Clim.* **26**, 710–725 (2013).
54. Udy, D. G., Vance, T. R., Kiem, A. S. & Holbrook, N. J. A synoptic bridge linking sea salt aerosol concentrations in East Antarctic snowfall to Australian rainfall. *Commun. Earth Environ.* **3**, 1–11 (2022).
55. Erickson, D. J., Merrill, J. T. & Duce, R. A. Seasonal estimates of global atmospheric sea-salt distributions. *J. Geophys. Res.: Atmos.* **91**, 1067–1072 (1986).
56. Gong, S. L. et al. Modeling sea-salt aerosols in the atmosphere: 2. Atmospheric concentrations and fluxes. *J. Geophys. Res.: Atmos.* **102**, 3819–3830 (1997).
57. Bushfire - Black Christmas, 2001 | Australian Disaster Resilience Knowledge Hub. <https://knowledge.aidr.org.au/resources/bushfire-black-christmas-2001/>.
58. Reeder, M. J., Spengler, T. & Musgrave, R. Rossby waves, extreme fronts, and wildfires in southeastern Australia. *Geophys. Res. Lett.* **42**, 2015–2023 (2015).
59. Parker, T. J., Berry, G. J. & Reeder, M. J. The structure and evolution of heat waves in Southeastern Australia. *J. Clim.* **27**, 5768–5785 (2014).
60. Black, M. T. & Lane, T. P. An improved diagnostic for summertime rainfall along the eastern seaboard of Australia. *Int. J. Climatol.* **35**, 4480–4492 (2015).
61. Taschetto, A. S. & England, M. H. An analysis of late twentieth century trends in Australian rainfall. *Int. J. Climatol.* **29**, 791–807 (2009).
62. Barnes, M. A., King, M., Reeder, M. & Jakob, C. The dynamics of slow-moving coherent cyclonic potential vorticity anomalies and their links to heavy rainfall over the eastern seaboard of Australia. *Q. J. R. Meteorol. Soc.* **149**, 2233–2251 (2023).
63. Black, R. X. & McDaniel, B. A. Interannual variability in the Southern hemisphere circulation organized by stratospheric final warming events. *J. Atmos. Sci.* **64**, 2968–2974 (2007).
64. Lim, E.-P., Hendon, H. H. & Thompson, D. W. J. Seasonal evolution of stratosphere-troposphere coupling in the southern hemisphere and implications for the predictability of surface climate. *J. Geophys. Res.: Atmos.* **123**, 12,002–12,016 (2018).
65. Ellis, S., Kanowski, P. & Whelan, R. National Inquiry into Bushfire Mitigation and Management, Council of Australian Governments, p. 451 Available online: <https://ro.uow.edu.au/scipapers/4/> (Commonwealth of Australia, 2004).
66. Rubino, M. et al. Revised records of atmospheric trace gases CO₂, CH₄, N₂O, and $\delta^{13}\text{C}-\text{CO}_2$ over the last 2000 years from Law Dome, Antarctica. *Earth Syst. Sci. Data* **11**, 473–492 (2019).
67. Mooney, S. D. et al. Late Quaternary fire regimes of Australasia. *Quat. Sci. Rev.* **30**, 28–46 (2011).
68. Palmer, J. G. et al. Drought variability in the eastern Australia and New Zealand summer drought atlas (ANZDA, CE 1500–2012) modulated by the Interdecadal Pacific Oscillation. *Environ. Res. Lett.* **10**, 124002 (2015).
69. Abram, N. J. et al. Evolution of the Southern Annular Mode during the past millennium. *Nat. Clim. Change* **4**, 564–569 (2014).
70. King, J., Anchukaitis, K. J., Allen, K., Vance, T. & Hessler, A. Trends and variability in the Southern Annular Mode over the Common Era. *Nat. Commun.* **14**, 2324 (2023).
71. McKay, R. C., Arblaster, J. M., Hope, P. & Lim, E.-P. Exploring atmospheric circulation leading to three anomalous Australian spring heat events. *Clim. Dyn.* **56**, 2181–2198 (2021).
72. McKay, R. C., Arblaster, J. M. & Hope, P. Tropical influence on heat-generating atmospheric circulation over Australia strengthens through spring. *Weather Clim. Dyn.* **3**, 413–428 (2022).

73. Marshall, A. G., Hudson, D., Wheeler, M. C., Hendon, H. H. & Alves, O. Simulation and prediction of the Southern Annular Mode and its influence on Australian intra-seasonal climate in POAMA. *Clim. Dyn.* **38**, 2483–2502 (2012).
74. Gergis, J., Neukom, R., Gallant, A. J. E. & Karoly, D. J. Australasian temperature reconstructions spanning the last millennium. *J. Clim.* **29**, 5365–5392 (2016).
75. Clarke, H. G. et al. Regional signatures of future fire weather over eastern Australia from global climate models. *Int. J. Wildland Fire* **20**, 550–562 (2011).
76. Squire, D. T. et al. Likelihood of unprecedented drought and fire weather during Australia's 2019 megafires. *npj Clim. Atmos. Sci.* **4**, 1–12 (2021).
77. CURRAN, M. et al. The Law Dome ice core 2000 year dataset collection. <https://doi.org/10.26179/5zm0-v192> (2021).
78. Roberts, J. et al. A 2000-year annual record of snow accumulation rates for Law Dome, East Antarctica. *Clim* **11**, 697–707 (2015).
79. van Ommen, T. D. & Morgan, V. Snowfall increase in coastal East Antarctica linked with southwest Western Australian drought. *Nat. Geosci.* **3**, 267 (2010).
80. Masson-Delmotte, V. et al. Recent southern Indian Ocean climate variability inferred from a Law Dome ice core: new insights for the interpretation of coastal Antarctic isotopic records. *Clim. Dyn.* **21**, 153–166 (2003).
81. Kiem, A. S. et al. Learning from the past – Using palaeoclimate data to better understand and manage drought in South East Queensland (SEQ), Australia. *J. Hydrol.: Reg. Stud.* **29**, 100686 (2020).
82. Vance, T. R. et al. Pacific decadal variability over the last 2000 years and implications for climatic risk. *Commun. Earth Environ.* **3**, 33 (2022).
83. Udy, D., Vance, T. R., Kiem, A., Holbrook, N. & Curran, M. Daily synoptic weather types of southern Indian Ocean: January 1979–October 2018. <https://doi.org/10.4225/15/58eedf00d78fe> (2020).
84. Noble, I. R., Gill, A. M. & Bary, G. V. McArthur's fire-danger meters expressed as equations. *Aust. J. Ecol.* **5**, 201–203 (1980).
85. Jones, D. A., Wang, W. & Fawcett, R. High-quality spatial climate data-sets for Australia. *Aust. Meteorol. Oceanogr. J.* **58**, 233 (2009).
86. Kalnay, E. et al. The NCEP/NCAR 40-year reanalysis project. in *Renew. Energy Vol1_146–Vol1_194* (Routledge, 2018).
87. Holgate, C. M., Van Dijk, A. I., Cary, G. J. & Yebra, M. Using alternative soil moisture estimates in the McArthur Forest Fire Danger Index. *Int. J. Wildland Fire* **26**, 806–819 (2017).
88. Australian Bureau of Meteorology. Australian Gridded Climate Data (AGCD) / AWAP v1.0.0 Snapshot (1900-01-01 to 2018-12-31). Downloaded from <https://doi.org/10.4227/166/5a8647d1c23e0> in May 2021. (2019).
89. Hersbach, H. et al. The ERA5 global reanalysis. *Q. J. R. Meteorol. Soc.* **146**, 1999–2049 (2020).
90. Nolan, R. H. et al. Predicting dead fine fuel moisture at regional scales using vapour pressure deficit from MODIS and gridded weather data. *Remote Sens. Environ.* **174**, 100–108 (2016).
91. Rakich, C. S., Holbrook, N. J. & Timbal, B. A pressure gradient metric capturing planetary-scale influences on eastern Australian rainfall. *Geophys. Res. Lett.* **35** <https://doi.org/10.1029/2007GL032970> (2008).
92. Marshall, G. J. Trends in the Southern Annular Mode from observations and reanalyses. *J. Clim.* **16**, 4134–4143 (2003).
93. Bureau of Meteorology. ENSO wrap up: Southern Oscillation Index (SOI) since 1876. <http://www.bom.gov.au/climate/enso/soi/> (Commonwealth of Australia, 2024). Accessed 5th June 2024.
94. Wilks, D. S. The stippling shows statistically significant grid points: How research results are routinely overstated and overinterpreted, and what to do about it. *Bull. Am. Meteorol. Soc.* **97**, 2263–2273 (2016).
95. Tozer, C. R. et al. Reconstructing pre-instrumental streamflow in Eastern Australia using a water balance approach. *J. Hydrol.* **558**, 632–646 (2018).
96. Tozer, C. R. et al. An ice core derived 1013-year catchment-scale annual rainfall reconstruction in subtropical eastern Australia. *Hydrol. Earth Syst. Sci.* **20**, 1703–1717 (2016).
97. Meehl, G. A., Teng, H., Maher, N. & England, M. H. Effects of the Mount Pinatubo eruption on decadal climate prediction skill of Pacific sea surface temperatures. *Geophys. Res. Lett.* **42**, 10,840–10,846 (2015).
98. Benassai, S. et al. Sea-spray deposition in Antarctic coastal and plateau areas from ITASE traverses. *Ann. Glaciol.* **41**, 32–40 (2005).
99. Iizuka, Y. et al. The rates of sea salt sulfatization in the atmosphere and surface snow of inland Antarctica. *J. Geophys. Res.: Atmos.* **117** <https://doi.org/10.1029/2011JD016378> (2012).
100. Duc, L. & Sawada, Y. A signal-processing-based interpretation of the Nash–Sutcliffe efficiency. *Hydrol. Earth Syst. Sci.* **27**, 1827–1839 (2023).
101. Montoya, D. *Bushfires in NSW: Timelines and Key Sources* <https://apo.org.au/node/40238> (2014).

Acknowledgements

We thank EunPa Lim and Andrew Dowdy from the Australian Bureau of Meteorology for access to datasets (stratospheric vortex and FFDI) and feedback on early versions of this research. We also thank all other researchers who made their palaeoclimate datasets publicly available, which aided the research we present here. Also, thanks to Brett Murphy for the 2019/20 burnt area dataset. DU, TV, AK, and NA acknowledge support from an ARC Discovery Project (DP220100606). DU and TV also acknowledge support from the Australian Antarctic Program Partnership (ASCI000002). DU, NH, and NA acknowledge support from the ARC Centre of Excellence for Climate Extremes (CE170100023). DU and NA also acknowledge support from the Australian Centre for Excellence in Antarctic Science (SR200100008). Analysis was undertaken with assistance from the National Computational Infrastructure (NCI), supported by the Australian Government. This work contributes to Australian Antarctic Science projects 4061, 4062, 4414, 4537, and 4630. We thank the editors, Rachel Rhodes and Alienor Lavergne, and reviewers (Scott Mooney and 2 anonymous) for their suggestions to improve the manuscript.

Author contributions

Danielle Udy conceived, designed, and led the study, undertaking the majority of the data analysis, interpretation, and writing of the manuscript. Tessa Vance developed the 2000-year LDSS timeseries. Tessa Vance, Anthony Kiem, Neil Holbrook, and Nerlie Abram all contributed substantially and equally to the data interpretation and critically revising the manuscript.

Competing interests

The authors declare no competing interests.

Additional information

Supplementary information The online version contains supplementary material available at <https://doi.org/10.1038/s43247-024-01470-z>.

Correspondence and requests for materials should be addressed to Danielle G. Udy.

Peer review information *Communications Earth & Environment* thanks Doug Richardson, Scott Mooney, and the other, anonymous, reviewer(s) for their contribution to the peer review of this work. Primary Handling Editors: Rachael Rhodes, Alienor Lavergne, and Carolina Ortiz Guerrero. A peer review file is available.

Reprints and permissions information is available at <http://www.nature.com/reprints>

Publisher's note Springer Nature remains neutral with regard to jurisdictional claims in published maps and institutional affiliations.

Open Access This article is licensed under a Creative Commons Attribution 4.0 International License, which permits use, sharing, adaptation, distribution and reproduction in any medium or format, as long as you give appropriate credit to the original author(s) and the source, provide a link to the Creative Commons licence, and indicate if changes were made. The images or other third party material in this article are included in the article's Creative Commons licence, unless indicated otherwise in a credit line to the material. If material is not included in the article's Creative Commons licence and your intended use is not permitted by statutory regulation or exceeds the permitted use, you will need to obtain permission directly from the copyright holder. To view a copy of this licence, visit <http://creativecommons.org/licenses/by/4.0/>.

© The Author(s) 2024